

## Article

# Designing Black Phosphorus and Heptazine-Based Crystalline Carbon Nitride Composites for Photocatalytic Water Splitting

Zijie Xiao <sup>1</sup>, Yayun Wang <sup>1</sup>, Hui Chen <sup>1</sup>, Haotian Wang <sup>1</sup>, Yuke Li <sup>2</sup>, Yilin Chen <sup>1,\*</sup> and Yun Zheng <sup>1,\*</sup> 

<sup>1</sup> Xiamen Key Laboratory of Optoelectronic Materials and Advanced Manufacturing, College of Materials Science and Engineering, Huaqiao University, Xiamen 361021, China

<sup>2</sup> Department of Chemistry and Centre for Scientific Modeling and Computation, Chinese University of Hong Kong, Hong Kong, China

\* Correspondence: ylchen@hqu.edu.cn (Y.C.); zheng-yun@hqu.edu.cn (Y.Z.)

**Abstract:** Black phosphorus (BP) and heptazine-based crystalline carbon nitride (KPHI) composite photocatalysts were synthesized by molten salt and ultrasound-assisted liquid phase exfoliation methods. The structure, morphology and optical properties of the as-prepared BP/KPHI composites were evaluated by various characterization techniques. In addition, the photocatalytic performance of BP/KPHI composites for hydrogen production was investigated. The photocatalytic activity of BP/KPHI composite catalysts could be modulated by changing the loading mass ratio of BP. The BP/KPHI composite photocatalyst with a mass ratio of 10% exhibited the highest photocatalytic activity with the hydrogen production rate of 4.3 mmol g<sup>-1</sup> h<sup>-1</sup>, about three times higher than that of pristine KPHI. Benefiting from the advantages of simplicity, rapidity, high yield and good controllability, this nanocomposite photocatalyst has the potential to serve as an excellent photocatalytic material for solar energy conversion.

**Keywords:** photocatalysis; hydrogen production; carbon nitride; black phosphorus; molten salt method



**Citation:** Xiao, Z.; Wang, Y.; Chen, H.; Wang, H.; Li, Y.; Chen, Y.; Zheng, Y. Designing Black Phosphorus and Heptazine-Based Crystalline Carbon Nitride Composites for Photocatalytic Water Splitting. *Crystals* **2023**, *13*, 312. <https://doi.org/10.3390/cryst13020312>

Academic Editors: Sibow Wang, Guangzhao Wang and Tingwei Zhou

Received: 21 December 2022

Revised: 2 February 2023

Accepted: 7 February 2023

Published: 14 February 2023



**Copyright:** © 2023 by the authors. Licensee MDPI, Basel, Switzerland. This article is an open access article distributed under the terms and conditions of the Creative Commons Attribution (CC BY) license (<https://creativecommons.org/licenses/by/4.0/>).

## 1. Introduction

Environmental and energy issues constitute a dual problem for civilization today due to the worldwide reliance on non-renewable fossil fuels and rising concern about their influence on the climate. It is both an essential requirement and a fantastic ambition to power our progress with sustainable resources. There is a great need for hydrogen, a fuel made from two earthly elements that are renewable: water and sunlight. With the high energy density, clean and pollution-free characteristics, hydrogen is considered as an ideal carrier of future energy. Photocatalytic decomposition of water for hydrogen production, which uses solar energy and photocatalyst to drive the decomposition reaction of water to produce hydrogen, has been considered to be one of the most ideal technologies for hydrogen production [1–4]. The design and preparation of low-cost and earth-abundant photocatalyst is of great importance to scale up photocatalytic water splitting for renewable hydrogen generation. The effective utilization of visible photons (400–700 nm), which make up approximately half of the solar energy that reaches the Earth's surface, is one of the biggest problems. Yet, conventional semiconductor materials suffer from low light utilization rate and easy recombination of photoinduced electrons and holes, which severely limit their practical applications in photocatalytic decomposition of water for the production of hydrogen [5–7]. Therefore, the design and fabrication of photocatalysts with high quantum efficiency and high solar energy utilization rate have become the most central problem in the field of photocatalysis at this stage [8].

Inorganic semiconductor photocatalysts (mainly metal oxides) have stimulated significant research interests over the past fifty years, however, the problem of inflexible regulation of the parameters restricted their practical applications. Conjugated polymer semiconductors may have the benefit of being simple to modify by synthetic control. Organic materials

are desirable substitutes for inorganic semiconductor photocatalysts due to their tunability and performance in versatile applications, including solar cells, photoelectrochemical devices, and light-emitting diodes. Polymeric carbon nitrides, sometimes referred to as melon, are promising photocatalysts for the decomposition of water for hydrogen production. A portion of visible light is absorbed, and the photogenerated charge carriers (electrons and holes) can be used in subsequent redox reactions, such as water splitting. It has been shown lately that the molten salt method can alleviate the structural defects and order of polymeric carbon nitrides. The molten salts in the process are in the solution state, which can control the specific rearrangement of its morphology and can also be used to change the condensation degree of the crystals. Because of their high photo-availability and a small degree of charge carrier recombination, crystalline carbon nitride has been found to have superior photocatalytic activity [9]. Heptazine-based crystalline carbon nitride, abbreviated as KPHI, was synthesized by the molten salt method. However, they also have certain disadvantages, such as a wide band gap, moderate utilization of visible light and low separation efficiency of photogenerated carriers, which lead to a certain limitation of the photocatalytic activity [10]. Therefore, it is necessary to improve the structure and surface properties of crystalline carbon nitride by mesoporosity, compounding, doping, organic copolymerization, and other means to overcome the above disadvantages.

Black phosphorus (BP), also known as phosphorene, is an emerging single-element two-dimensional (2D) material that has recently attracted significant attention [11,12]. BP has intriguing properties, such as layer-dependent direct band gap, strong visible and near-infrared light absorption, high carrier mobility, in-plane structural anisotropy, low toxicity, and biocompatibility. Based on these properties, BP has the potential to function as a catalyst for water splitting and other photoredox processes. However, a BP photocatalyst also has drawbacks, such as rapid recombination of photoexcited electron-holes and low stability. Therefore, it only shows moderate catalytic activity in many photocatalytic processes [13–15]. To solve these problems, building heterostructured photocatalysts based on BP can prevent the recombination of photogenerated charge and carriers and greatly increase photocatalytic activity [16]. Thus, BP-based heterostructured photocatalysts can be used by combining the advantages of high carrier mobility and broad-spectrum absorption capability. It is noted that both BP and KPHI materials could be exfoliated into few-layered and graphene-like two-dimensional nanosheets. The composite of KPHI and BP could constitute a two-dimensional/two-dimensional (2D/2D) heterostructure. This can effectively promote the effective electron-hole transfer between them and reduce the recombination of photoinduced charge carriers [17]. Thus, the efficiency of photocatalytic hydrogen production from water can be improved [18–23].

In this study, KPHI/BP nanocomposites were prepared by molten salt method and ultrasound-assisted liquid exfoliation approach. The catalysts were evaluated by scanning electron microscopy (SEM), transmission electron microscopy (TEM), and energy dispersive spectroscopy (EDS), X-ray powder diffraction (XRD), Fourier transform infrared spectroscopy (FT-IR), UV-vis diffuse reflectance spectroscopy (DRS), and photoluminescence (PL) spectroscopy. In addition, the performance of the prepared catalysts for photolysis of water to produce hydrogen gas was investigated.

## 2. Materials and Methods

### 2.1. Chemical Reagents

Melamine ( $C_3H_6N_6$ ), lithium chloride (LiCl), potassium chloride (KCl), N-Methylpyrrolidone ( $C_5H_9NO$ ), ethanol ( $C_2H_5OH$ ), methanol ( $CH_3OH$ ), and triethanolamine ( $C_6H_{15}NO_3$ ) were bought from Aladdin Biochemical Technology Co., Ltd. (Shanghai, China). All reagents used are analytically pure for the study. The above reagents do not need to be purified once again and can be used directly.  $H_2PtCl_6 \cdot 6H_2O$  (Pt > 37%) was achieved from the China Sinopharm Chemical Reagent Co., Ltd. (Shanghai, China). Black phosphorus (BP) crystal powder (>99.998%) was purchased from Nanjing Xianfeng Nano Material Technology Co., Ltd. (XFNANO, Nanjing, China). Nitrogen ( $N_2$ ) and Argon (Ar) gas were obtained from

Fujian Nanan Chenggong Gas Co., Ltd. (Fujian, China). Deionized water was used in the experimental procedure.

## 2.2. Fabrication of Materials

### 2.2.1. Fabrication of KPHI

Crystalline carbon nitride was prepared by the molten salt method. 8 g of melamine was weighed into a porcelain boat. Then it was placed in a tube furnace at a temperature of 500 °C (constant temperature for 4 h) and cooled to room temperature. 600 mg powder sample was weighed and ground with 3.3 g KCl and 2.7 g LiCl, and the mixture was placed in a tube furnace. It was heated to 550 °C (nitrogen atmosphere, heating rate of 2 °C/min) at a constant temperature for 4 h. The calcined sample was placed in a beaker with a small amount of deionized water and ultrasonically dispersed for 5 min. It was filtered for several times to remove KCl and LiCl. The samples were placed in a vacuum drying oven at 70 °C for 8 h. After cooling to room temperature, the sample was ground to obtain a solid powder. The solid powder sample is KPHI.

### 2.2.2. Fabrication of BP/KPHI

Synthesis using ultrasonic-assisted liquid exfoliation method: 0.2 g of crystalline carbon nitride was weighed on an analytical balance, and 20 mL of N-methylpyrrolidone was measured in a 50 mL measuring cylinder. Subsequently, BP in mass ratios of 1%, 5%, 10%, 15% and 20% was added in a 50 mL centrifuge tube. The centrifuge tubes were placed in a thermostatic glass vessel with a circulating water temperature of 5 °C, mixed and put into ultrasonic pulverization. The mixtures were sonicated for 24 h. After homogeneous mixing, the complexes were washed by centrifugation with ethanol as a solution, and the liquid was separated by centrifugation. Finally, the two-dimensional composites of KPHI with different BP mass ratios were obtained.

## 2.3. Characterization

Morphological studies of the synthesized nanomaterials were carried out by scanning electron microscopy (Hitachi Co., Tokyo, Japan, Hitachi S-4800). In addition, transmission electron microscopy (JEOL Co., Tokyo, Japan, JEM 2010 EX 300) was used for morphological observation of the prepared samples, and energy dispersive X-ray spectrometer was used to analyze the chemical composition of the photocatalytic materials. X-ray powder diffraction analysis was performed on the nanomaterials using an x-ray diffractometer (Rigaku Co., Tokyo, Japan, Smart lab) equipped with a Cu K $\alpha$  radiation source ( $\lambda = 1.5418 \text{ \AA}$ ) to study their structural properties. The Fourier transform infrared spectrophotometer (Nicolet, Madison, USA, Nicolet iS10) was used to determine each functional group. X-ray photoelectron spectroscopy was tested on an instrument (Thermo Scientific, Waltham, MA, USA, ESCALAB250) with a monochromatized Al K $\alpha$  line source (200 W). All binding energies were referenced to the C 1s peak at 284.8 eV of surface adventitious carbon. A UV-vis spectrophotometer (Shimadzu Co., Kyoto, Japan, UV-2550) was used to detect the optical properties of the synthesized nanomaterials while recording the absorption spectra in the range of 350–550 nm. Photoluminescence (Edinburgh Co., Edinburgh, UK, FLS920) spectra were studied using a fluorescence spectrophotometer.

## 2.4. Photocatalytic Activity

The test system used in this experiment mainly consists of a closed gas circulation-evacuation system (Figure S1, see Supplementary Materials, Ceaulight CEL-SPH2N, Beijing, China), and a low-temp thermostatic water bath (DC-1006, Hinotek, Zhejiang, China), and a gas chromatograph (Shimadzu Co., Kyoto, Japan, GC-2014C, thermal conductivity detector, 5A, sieve, high purity Ar as carrier gas). A 300 W Xenon lamp (Perfect Light PLSSXE, Beijing, China) was used as the light source with >420 nm light irradiation. In order to keep the temperature of the system constant, circulating cooling water was used. 50 mg BP/KPHI (10 wt.% mass ratio) catalyst, 80 mL deionized water, 20 mL methanol (sacrificial

agent), and chloroplatinic acid solution (containing 3 wt.% Pt) were mixed and sonicated for five minutes in a glass reaction vessel with a volume of 350 mL. An in-situ photodeposition approach employing chloroplatinic acid as the precursor was used to deposit Pt co-catalyst on the sample surface. After that, the system is sealed and the gas is removed. Then the photoirradiation was continued for 5 h. During the experiment, the gas chromatograph was used to detect the hydrogen amount every hour.

### 3. Results and Discussion

#### 3.1. Morphology Characterization of Catalysts

In this experiment, SEM, TEM, and EDS spectra were recorded for the preliminary characterization of the morphology for the catalyst. Figure 1 shows the SEM image of 10% BP/KPHI composite photocatalyst. It can be found that in the 10% BP/KPHI complex, the flat-layered BP nanosheets combined well with the KPHI nanosheets with apparent stacking pore structures. The elemental mapping and EDS results of the BP/KPHI composite further demonstrate the presence of C, N, P, K, O, and Cl elements (Figures 2 and 3). Furthermore, the actual mass fraction of BP is *ca.* 11% for 10% BP/KPHI catalyst (Table S1).

In order to elucidate the composition and chemical structure of the composite photocatalysts of BP/KPHI with different mass ratios, the catalysts were examined by using XPS, XRD, and FT-IR. Figure 4 shows the XRD patterns of BP/KPHI composite photocatalysts with mass ratios of 5%, 10%, 15% and 20%, respectively. The two diffraction peaks are attributed to BP/KPHI composite photocatalysts with (002) crystalline planes at  $8.1^\circ$  and  $27.5^\circ$ . The periodically repeating heptazine units within the facets lead to the former peak [24–26]. Moreover, the latter diffraction peak is attributed to a layered stacking of heptazine structures similar to graphite. It was confirmed that the prepared product contains heptazine-based graphite-like carbon nitride. The BP/KPHI composite photocatalyst showed three different XRD diffraction peaks at  $16.9^\circ$ ,  $26.5^\circ$ ,  $34.2^\circ$ ,  $35.0^\circ$ , and  $52.3^\circ$ . This is caused by the (020), (021), (040), (111), and (060) crystal planes of BP. These results confirm the presence of BP/KPHI composite photocatalyst. The crystalline diffraction peaks of BP are gradually enhanced with the increased BP mass ratio in the composite photocatalyst.

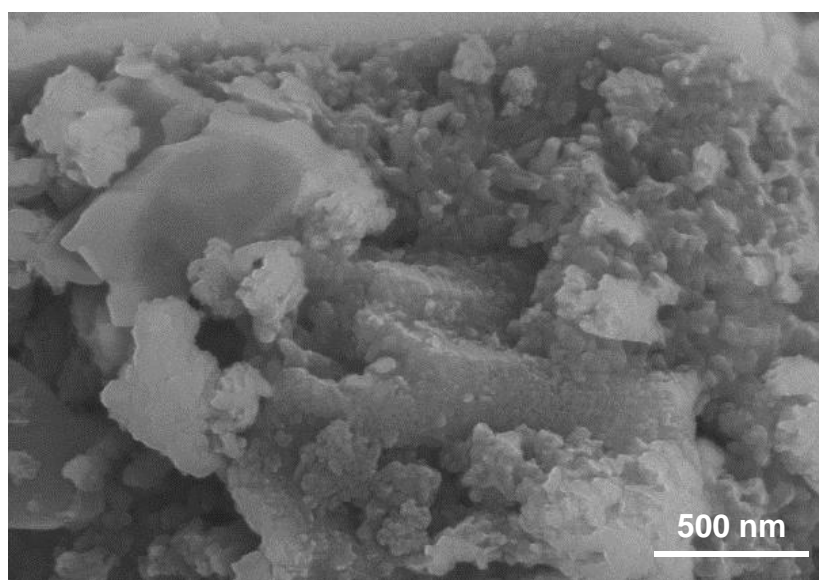
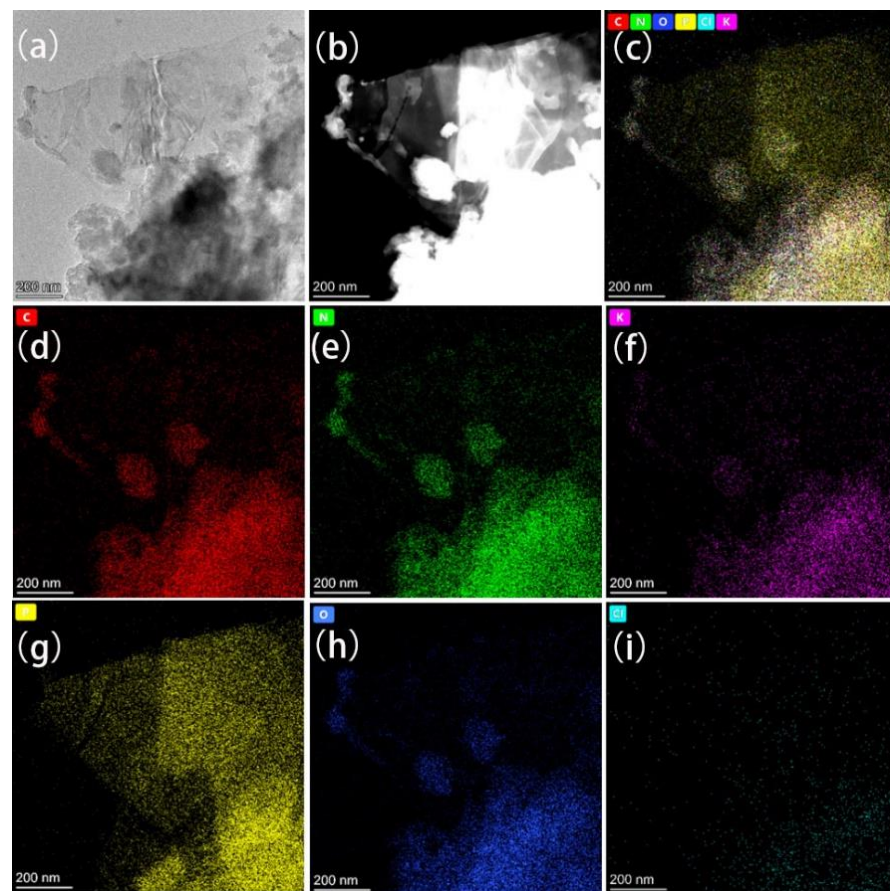
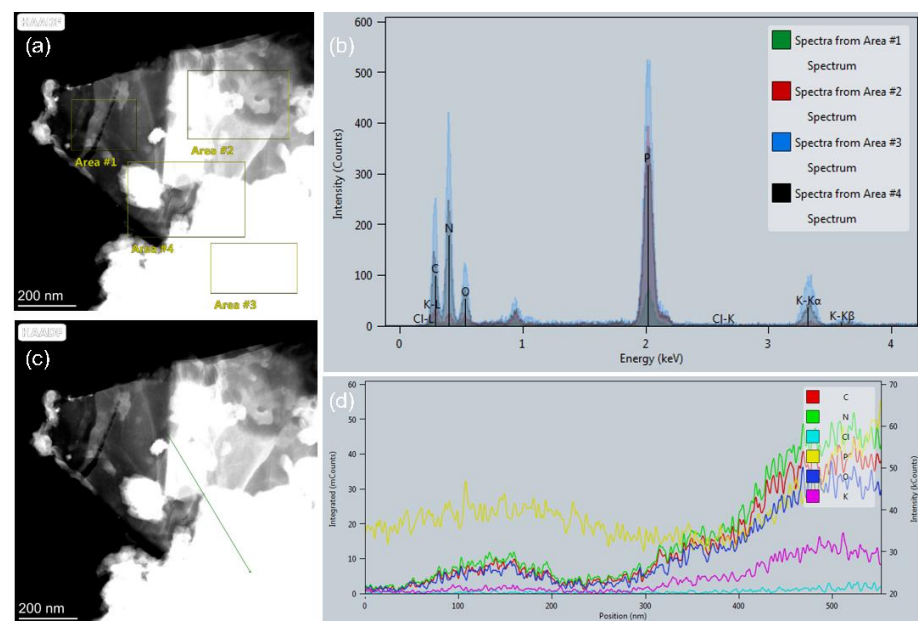


Figure 1. SEM images of 10% BP/KPHI.



**Figure 2.** (a) TEM image of 10%BP/KPHI; (b) Dark field TEM image of 10%BP/KPHI; high-angle annular dark-field TEM element mapping images of 10%BP/KPHI catalyst. (c) all elements, (d) for C, (e) for N, (f) for K, (g) for P, (h) for O, and (i) for Cl.



**Figure 3.** (a,c) TEM image of 10%BP/KPHI; (b) EDS image of 10%BP/KPHI; (d) Line scanning profile of 10%BP/KPHI catalyst.

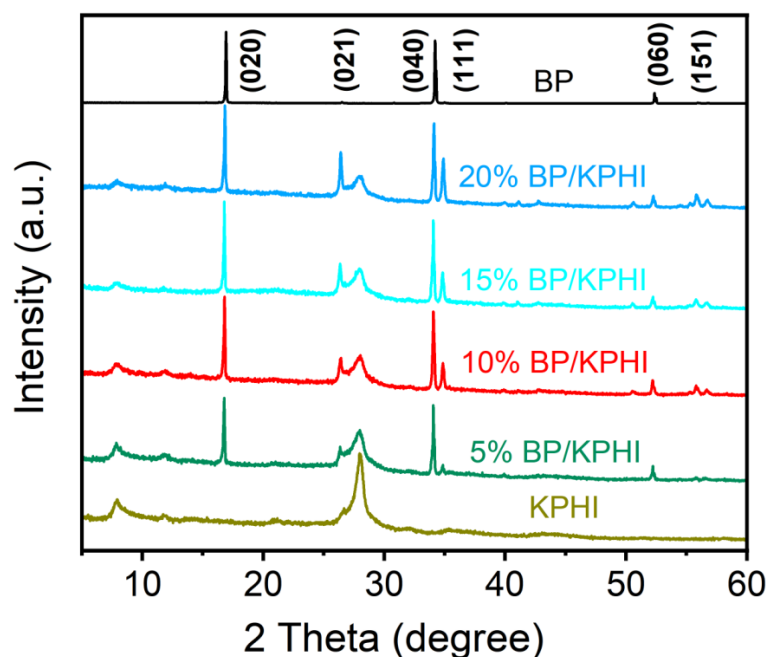


**Figure 4.** XRD patterns of KPHI, 5%BP/KPHI, 10%BP/KPHI, 15%BP/KPHI, 20%BP/KPHI, and BP.

Figure 5 shows the FT–IR spectra of the composite photocatalysts of BP/KPHI with mass ratios of 5%, 10%, 15%, and 20%. A moderate intensity absorption peak caused by the stretching vibration of the heptazine ring at  $1200\text{--}1700\text{ cm}^{-1}$  and a fingerprint vibration peak attributed to the heptazine ring at  $810\text{ cm}^{-1}$  could be seen in the figure [27]. A broad absorption peak caused by the amine vibration of the surface is found near  $3000\text{ cm}^{-1}$ . In addition, there is a characteristic absorption peak at  $2170\text{ cm}^{-1}$  caused by the vibration of cyano group, probably due to the partial decomposition of the heptazine ring [28,29]. This figure indicates that the composite sample contains KPHI.

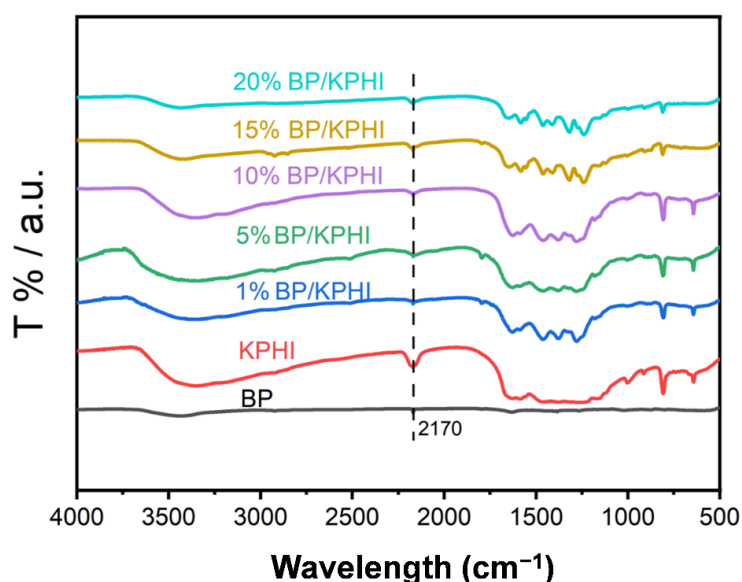


**Figure 5.** FT–IR spectra of BP/KPHI composites with different mass ratios, KPHI and BP.

In order to further analyze the surface composition and chemical bonding forms of the composite photocatalysts of BP/KPHI with mass ratios of 5%, 10%, 15%, and 20%, respectively, the prepared photocatalytic composite catalysts were characterized by X-ray photoelectron spectroscopy (XPS) during the experiments. The spectral peaks of five

elements, namely C, N, K, O, and P, can be observed in Figure 6. In the high-resolution spectrum of C 1s, there are three peaks at 284.8, 286.4, and 288.3 eV, respectively, with the strongest peak at 288.3 eV. The peaks at 286.4 and 288.3 eV mainly originate from the backbone structure of the polymeric carbon nitride, which is the  $sp^2$  hybridization of carbon atoms in the nitrogen-containing heterocyclic ring. The spectrum at 284.8 eV is generally attributed to the impurity of carbon. N 1s spectrum can be deconvoluted into four peaks, the one at 398.8 eV is attributed to the  $sp^2$  hybridization of the nitrogen atom in the heptazine ring (C-N=C), and the one at 400.5 eV is attributed to the ternary nitrogen N-(C)<sub>3</sub> in the heptazine ring. These two structures of carbon and nitrogen atoms are the main structure of the carbon nitride framework. The peak at 401.3 eV indicates the presence of an amino group (C-N-H) in the structure, which is mainly present on the surface of the sample. The peak at 404.1 eV, on the other hand, may be caused by nuclear or positive charge localization effects. No spectral peaks of Cl 2p and Li 1s were observed in the high-resolution spectra, which suggests that these elements have been removed after extensive deionized water washing [30–32]. Due to the presence of K ions in the synthesized carbon nitride, the resulting framework will be charge compensated in a manner similar to potassium melonate, which contains the structure of cyano group. This is consistent with the results described in the FT-IR spectra above. In the spectrum of P 2p, there are two peaks of typical P 2p binding energy of BP, attributed to P 2p<sub>3/2</sub> (129.0 eV) and P 2p<sub>1/2</sub> (130.0 eV). In the XPS spectrum, the peak for the O element was observed. This signal is mainly derived from the phosphorus oxide formed by the slight oxidation of BP surface for the sample.

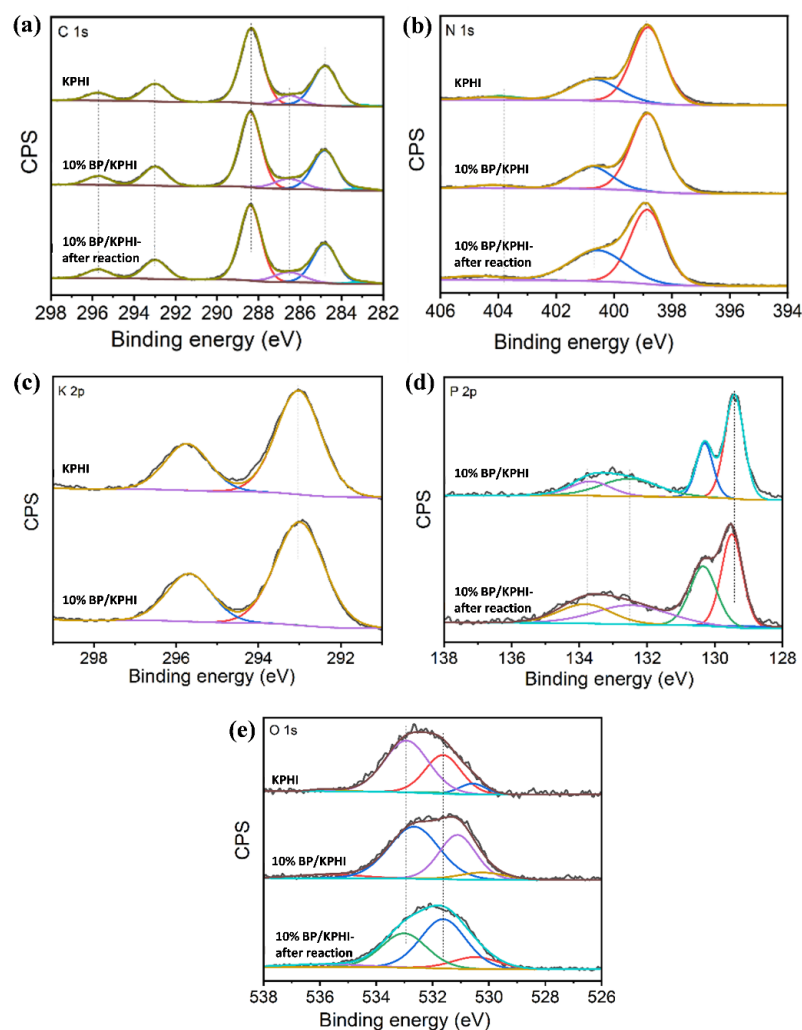
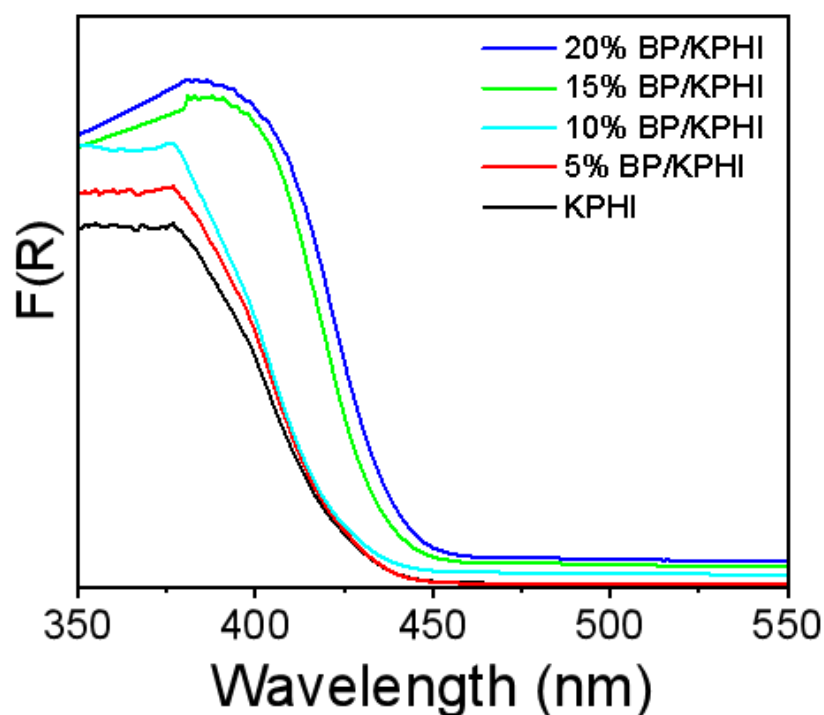


Figure 6. XPS spectra of (a) C 1s, (b) N 1s, (c) K 2p, (d) P 2p, and (e) O 1s for 10% BP/KPHI.

### 3.2. Optical Properties of Catalysts

Figure 7 shows the UV-vis DRS spectra of the BP/KPHI composite photocatalyst with mass ratios of 5%, 10%, 15%, and 20% and pristine KPHI, respectively. The KPHI samples exhibit typical semiconductor absorption properties. The absorption of incident light is vital for the photocatalytic process, which excites electrons from the valence band to the conduction band for the catalyst. The light absorption intensity of the BP/KPHI sample gradually enhances with increasing BP content, and the edge of the absorption band gradually redshifts. Thus the absorption and utilization ability of visible light increases, and more incident photon energy can be absorbed and utilized by the photocatalytic composite catalyst. Also, the 10% BP/KPHI has a narrower band gap than KPHI (Figure S2). Thus, its photocatalytic performance is significantly improved.



**Figure 7.** UV-vis DRS spectra of KPHI and KPHI/BP composite photocatalysts with different mass ratios.

### 3.3. Photocatalytic Activity

The visible light photocatalytic activity was further evaluated by testing the hydrogen production rate of KPHI/BP composite photocatalysts with different mass ratios of BP. In this system, 3 wt.% Pt co-catalyst was in-situ photodeposited onto the photocatalyst, and methanol was utilized as a sacrificial agent. Figure 8 compares the photocatalytic hydrogen production activity of BP/KPHI hybrids with different mass ratios. It can be found that there is low hydrogen production rate for pure BP. The composite photocatalysts of BP/KPHI showed significantly higher hydrogen production activity than pristine KPHI. With the increasing BP content, the hydrogen production rate of BP/KPHI composite photocatalyst raised significantly. When the BP content reaches 10%, the BP/KPHI composite photocatalyst exhibited the highest photocatalytic hydrogen production activity. The molarity of hydrogen produced for 10% BP/KPHI was  $21.5 \text{ mmol g}^{-1}$  after 5 h of light exposure, and the hydrogen production rate was  $4.3 \text{ mmol g}^{-1} \text{ h}^{-1}$ . However, when the adding amount of BP exceeded 10%, the photocatalytic hydrogen production activity of BP/KPHI composite photocatalysts began to decrease. The decreased photocatalytic hydrogen production activity was probably due to the shielding effect of the incident light by the excessive BP loading, which reduced the separation efficiency of photogenerated carriers.

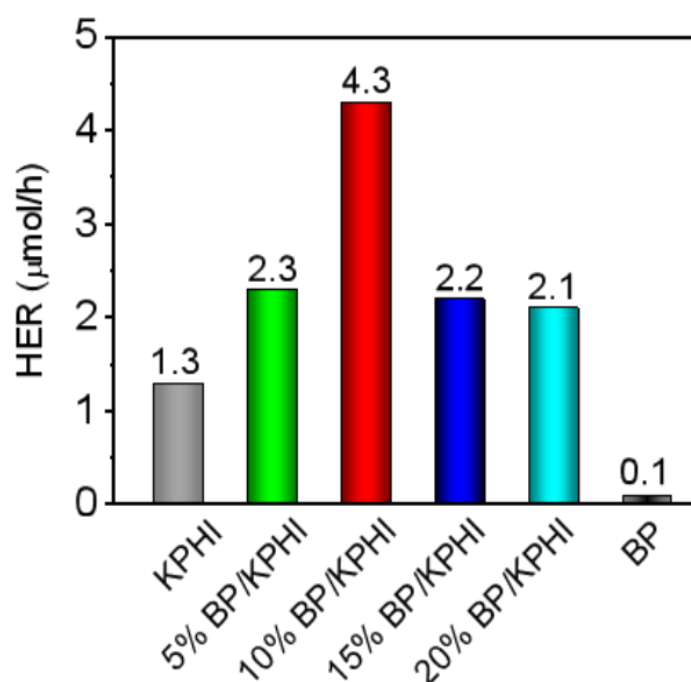


**Figure 8.** Average hydrogen evolution rate (HER) of 3 wt.% Pt-deposited KPHI and BP/KPHI illuminated by visible light ( $\lambda > 420$  nm) for 5 h.

Control experiments of photocatalytic hydrogen evolution were performed. No detectable amount of  $\text{H}_2$  was determined in the absence of catalyst, light or methanol (Table S2). The effect of other factors was excluded.

As shown in Figure 9, the apparent quantum yield (AQY) of 10% BP/KPHI composite photocatalyst decreased gradually with the increasing incident light wavelength, which was consistent with the trend of its UV-vis absorption spectrum (Figure 7). Among them, the AQY of hydrogen production of 10% BP/KPHI composite photocatalyst was 3.1% at 420 nm. It surpasses most of the previously reported catalysts in the paper (Table S3).

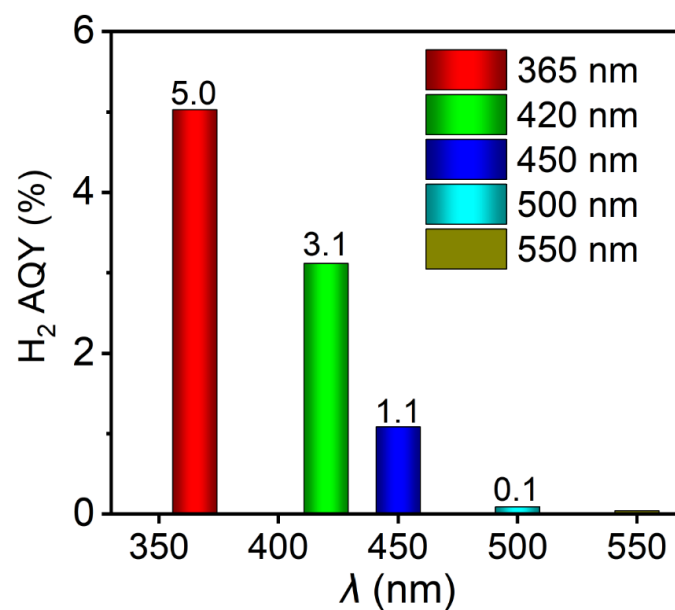


**Figure 9.** Wavelength-dependent AQYs of photocatalytic  $\text{H}_2$  production and the corresponding UV-vis DRS spectrum for 10% BP/KPHI.

Figure 10 shows the stability test of 10% BP/KPHI composite photocatalyst for hydrogen production reaction under visible light illumination ( $\lambda > 420$  nm) for 25 h. It can be seen from the figure that hydrogen production increased steadily with the increasing photoreaction time. Only small fluctuations were observed between each cycle. It indicates that 10% BP/KPHI composite sample has good stability in photocatalytic hydrogen production reaction.

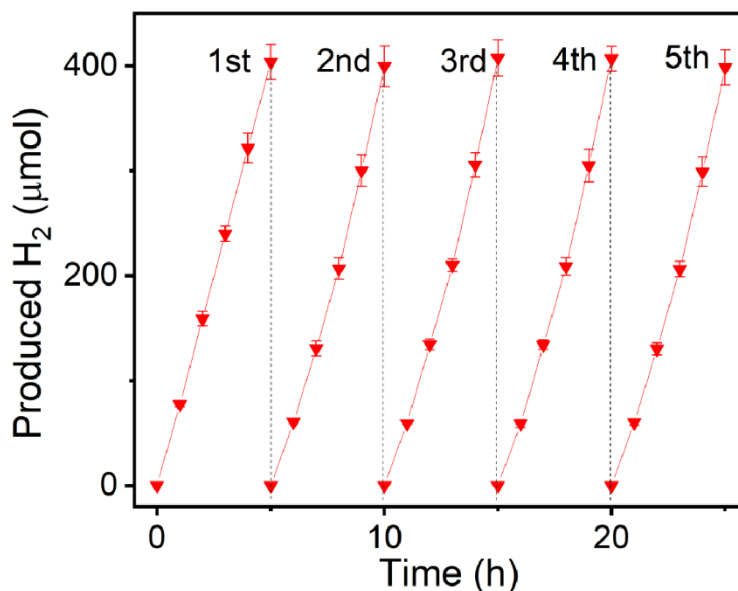


Figure 10. Reusability of 10% BP/KPHI catalyst for evolving H<sub>2</sub> over five successive experimental runs.

Figure 11 shows the XRD patterns of 10% BP/KPHI composite photocatalyst before and after the photocatalytic hydrogen production reaction. The peak positions and intensities of the 10% BP/KPHI composite photocatalysts did not change significantly before and after the photocatalytic decomposition of water reaction, indicating that 10% BP/KPHI catalyst has good stability during photocatalytic reactions.

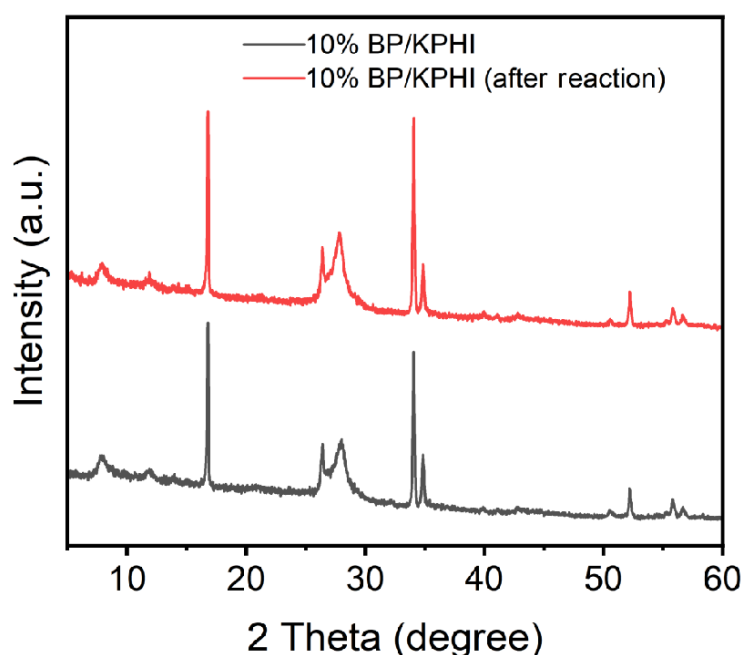


Figure 11. XRD patterns of 10%BP/KPHI and 10%BP/KPHI (after H<sub>2</sub> production reaction).

The photogenerated charge separation behavior of KPHI and BP/KPHI was investigated by photoluminescence (PL) spectroscopy. As displayed in Figure 12, KPHI and BP/KPHI composite photocatalysts show broad emission peak centered at about 475 nm. The figure shows that the fluorescence peak of pristine KPHI is stronger, and its photogenerated charge carriers recombine severely. In contrast, the fluorescence peak intensity of the BP/KPHI composite photocatalyst doping with BP is greatly reduced, indicating that it can effectively reduce the recombination probability of photogenerated charge carriers. However, when the loading ratio of BP exceeded 10%, the fluorescence peak intensity increased, indicating that excessive BP loading lead to higher recombination of photogenerated charge carriers.

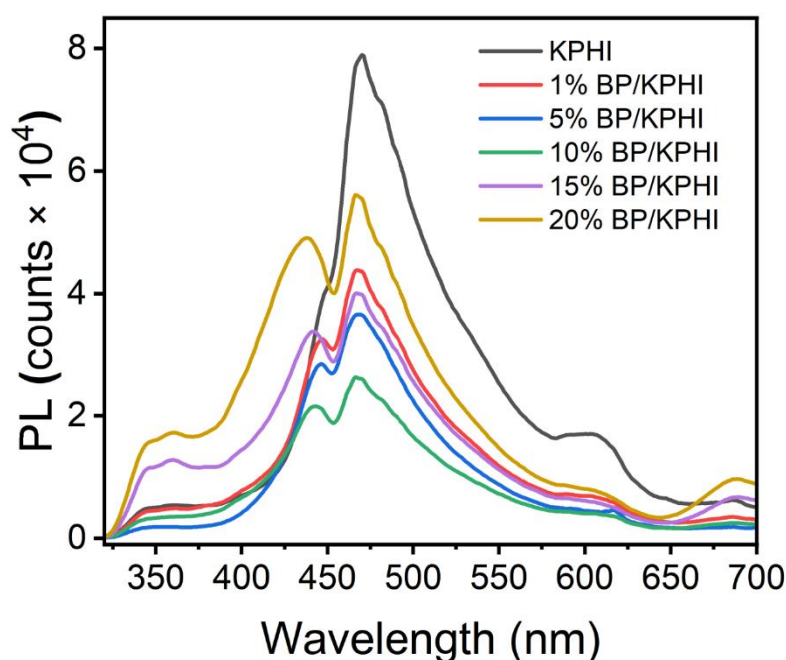


Figure 12. PL spectra of BP/KPHI and KPHI samples.

#### 4. Conclusions

In this study, black phosphorus and heptazine-based crystalline carbon nitride nanocomposites were prepared by molten salt and ultrasonic exfoliation methods. The hybrid of black phosphorus and heptazine-based crystalline carbon nitride could serve as an effective photocatalysts for water splitting with the highest hydrogen production rate of  $4.3 \text{ mmol g}^{-1} \text{ h}^{-1}$ , which is about three times higher than that of pristine crystalline carbon nitride. The superior photocatalytic activity of the hybrid is primarily attributed to the promoted separation of photoinduced charge carriers and enhanced visible light absorption ability. Owing to the benefits of simplicity, high-efficiency, cost-effectiveness, and superior controllability, the heterostructured photocatalysts have the potential to be a superior photocatalytic material for solar fuel production.

**Supplementary Materials:** The following supporting information can be downloaded at: <https://www.mdpi.com/article/10.3390/cryst13020312/s1>, Figure S1: Photocatalytic hydrogen production equipment (CEL-SPH2N system); Figure S2: Band gap energies of KPHI and 10% BP/KPHI; Table S1: Analysis result of EDS spectrum from 10% BP/KPHI; Table S2: Photocatalytic hydrogen production rate in the no-treatment control group; Table S3: Summary of the photocatalytic activities of BP-based photocatalysts for  $\text{H}_2$  evolution. References [33–39] are cited in the supplementary materials.

**Author Contributions:** Data curation, Z.X. and Y.W.; Funding acquisition, Y.Z.; Investigation, H.C. and H.W.; Project administration, Y.L. and Y.C.; Supervision, Y.C. and Y.Z.; Writing—original draft, Y.Z. and Z.X. All authors have read and agreed to the published version of the manuscript.

**Funding:** This research was funded by the National Natural Science Foundation of China (21902051), the Natural Science Foundation of Fujian Province (2019J05090), the Fundamental Research Funds for the Central Universities (ZQN-807), and the Graphene Powder and Composite Research Center of Fujian Province (2017H2001).

**Data Availability Statement:** Not applicable.

**Acknowledgments:** The authors thank Instrumental Analysis Center of Huaqiao University for XPS and UV-vis DRS analysis. The authors thank Shiyanjia Lab ([www.shiyanjia.com](http://www.shiyanjia.com)) for the TEM test.

**Conflicts of Interest:** The authors declare no conflict of interest.

## References

1. Wang, X.; Maeda, K.; Thomas, A.; Takahashi, K.; Xin, G.; Carlsson, J.M.; Domen, K.; Antonietti, M. A metal-free polymeric photocatalyst for hydrogen production from water under visible light. *Nat. Mater.* **2009**, *8*, 76–80. [[CrossRef](#)] [[PubMed](#)]
2. Damkale, S.R.; Arbuj, S.S.; Umarji, G.G.; Panmand, R.P.; Khore, S.K.; Sonawane, R.S.; Rane, S.B.; Kale, B.B. Two-dimensional hexagonal SnS<sub>2</sub> nanostructures for photocatalytic hydrogen generation and dye degradation. *Sustain. Energy Fuels* **2019**, *3*, 3406–3414. [[CrossRef](#)]
3. Li, J.; Yuan, H.; Zhang, W.; Jin, B.; Feng, Q.; Huang, J.; Jiao, Z. Advances in Z-scheme semiconductor photocatalysts for the photoelectrochemical applications: A review. *Carbon Energy* **2022**, *4*, 294–331. [[CrossRef](#)]
4. Ren, Y.; Dong, Y.; Feng, Y.; Xu, J. Compositing two-dimensional materials with TiO<sub>2</sub> for photocatalysis. *Catalysts* **2018**, *8*, 590. [[CrossRef](#)]
5. Wang, S.; Guan, B.Y.; Lou, X.W.D. Construction of ZnIn<sub>2</sub>S<sub>4</sub>–In<sub>2</sub>O<sub>3</sub> hierarchical tubular heterostructures for efficient CO<sub>2</sub> photoreduction. *J. Am. Chem. Soc.* **2018**, *140*, 5037–5040. [[CrossRef](#)]
6. Wang, B.; Liu, J.; Yao, S.; Liu, F.; Li, Y.; He, J.; Lin, Z.; Huang, F.; Liu, C.; Wang, M. Vacancy engineering in nanostructured semiconductors for enhancing photocatalysis. *J. Mater. Chem. A* **2021**, *9*, 17143–17172. [[CrossRef](#)]
7. Yang, L.; Peng, Y.; Luo, X.; Dan, Y.; Ye, J.; Zhou, Y.; Zou, Z. Beyond C<sub>3</sub>N<sub>4</sub>  $\pi$ -conjugated metal-free polymeric semiconductors for photocatalytic chemical transformations. *Chem. Soc. Rev.* **2021**, *50*, 2147–2172. [[CrossRef](#)]
8. Lewis, N.S. Research opportunities to advance solar energy utilization. *Science* **2016**, *351*, aad1920. [[CrossRef](#)] [[PubMed](#)]
9. Li, C.; Li, J.; Huang, Y.; Liu, J.; Ma, M.; Liu, K.; Zhao, C.; Wang, Z.; Qu, S.; Zhang, L.; et al. Recent development in electronic structure tuning of graphitic carbon nitride for highly efficient photocatalysis. *J. Semicond.* **2022**, *43*, 021701. [[CrossRef](#)]
10. Liao, G.; Gong, Y.; Zhang, L.; Gao, H.; Yang, G.-J.; Fang, B. Semiconductor polymeric graphitic carbon nitride photocatalysts: The “holy grail” for the photocatalytic hydrogen evolution reaction under visible light. *Energy Environ. Sci.* **2019**, *12*, 2080–2147. [[CrossRef](#)]
11. Zhao, G.-Q.; Hu, J.; Long, X.; Zou, J.; Yu, J.-G.; Jiao, F.-P. A critical review on black phosphorus-based photocatalytic CO<sub>2</sub> reduction application. *Small* **2021**, *17*, 2102155. [[CrossRef](#)] [[PubMed](#)]
12. Ren, X.; Philo, D.; Li, Y.; Shi, L.; Chang, K.; Ye, J. Recent advances of low-dimensional phosphorus-based nanomaterials for solar-driven photocatalytic reactions. *Coord. Chem. Rev.* **2020**, *424*, 213516. [[CrossRef](#)]
13. Zhou, M.; Wang, S.; Yang, P.; Huang, C.; Wang, X. Boron carbon nitride semiconductors decorated with CdS nanoparticles for photocatalytic reduction of CO<sub>2</sub>. *ACS Catal.* **2018**, *8*, 4928–4936. [[CrossRef](#)]
14. Bi, Q.; Hu, K.; Chen, J.; Zhang, Y.; Riaz, M.S.; Xu, J.; Han, Y.; Huang, F. Black phosphorus coupled black titania nanocomposites with enhanced sunlight absorption properties for efficient photocatalytic CO<sub>2</sub> reduction. *Appl. Catal. B* **2021**, *295*, 120211. [[CrossRef](#)]
15. Chen, C.; Hu, J.; Yang, X.; Yang, T.; Qu, J.; Guo, C.; Li, C.M. Ambient-stable black phosphorus-based 2D/2D S-scheme heterojunction for efficient photocatalytic CO<sub>2</sub> reduction to syngas. *ACS Appl. Mater. Interfaces* **2021**, *13*, 20162–20173. [[CrossRef](#)]
16. Zheng, Y.; Chen, Y.; Gao, B.; Lin, B.; Wang, X. Phosphorene-based heterostructured photocatalysts. *Engineering* **2021**, *7*, 991–1001. [[CrossRef](#)]
17. Zhu, M.; Kim, S.; Mao, L.; Fujitsuka, M.; Zhang, J.; Wang, X.; Majima, T. Metal-Free Photocatalyst for H<sub>2</sub> evolution in visible to near-infrared region: Black phosphorus/graphitic carbon nitride. *J. Am. Chem. Soc.* **2017**, *139*, 13234–13242. [[CrossRef](#)] [[PubMed](#)]
18. Zheng, Y.; Yu, Z.; Ou, H.; Asiri, A.M.; Chen, Y.; Wang, X. Black phosphorus and polymeric carbon nitride heterostructure for photoinduced molecular oxygen activation. *Adv. Funct. Mater.* **2018**, *28*, 1705407. [[CrossRef](#)]
19. Zheng, Y.; Chen, Y.; Wang, L.; Tan, M.; Xiao, Y.; Gao, B.; Lin, B. Metal-free 2D/2D heterostructured photocatalyst of black phosphorus/covalent triazine-based frameworks for water splitting and pollutant degradation. *Sustain. Energy Fuels* **2020**, *4*, 3739–3746. [[CrossRef](#)]
20. Liu, C.; Han, Z.; Feng, Y.; Dai, H.; Zhao, Y.; Han, N.; Zhang, Q.; Zou, Z. Ultrathin Z-scheme 2D/2D N-doped HTiNbO<sub>5</sub> nanosheets/g-C<sub>3</sub>N<sub>4</sub> porous composites for efficient photocatalytic degradation and H<sub>2</sub> generation under visible light. *J. Colloid Interface Sci.* **2021**, *583*, 58–70. [[CrossRef](#)] [[PubMed](#)]
21. Jia, J.; Sun, W.; Zhang, Q.; Zhang, X.; Hu, X.; Liu, E.; Fan, J. Inter-plane heterojunctions within 2D/2D FeSe<sub>2</sub>/g-C<sub>3</sub>N<sub>4</sub> nanosheet semiconductors for photocatalytic hydrogen generation. *Appl. Catal. B* **2020**, *261*, 118249. [[CrossRef](#)]

22. He, F.; Zhu, B.; Cheng, B.; Yu, J.; Ho, W.; Macyk, W. 2D/2D/0D TiO<sub>2</sub>/C<sub>3</sub>N<sub>4</sub>/Ti<sub>3</sub>C<sub>2</sub> MXene composite S-scheme photocatalyst with enhanced CO<sub>2</sub> reduction activity. *Appl. Catal. B* **2020**, *272*, 119006. [[CrossRef](#)]
23. Zheng, D.; Zhou, J.; Fang, Z.; Heil, T.; Savateev, A.; Zhang, Y.; Antonietti, M.; Zhang, G.; Wang, X. H<sub>2</sub> and CH<sub>4</sub> production from bio-alcohols using condensed poly(heptazine imide) with visible light. *J. Mater. Chem. A* **2021**, *9*, 27370–27379. [[CrossRef](#)]
24. Zhang, G.; Li, G.; Heil, T.; Zafeiratos, S.; Lai, F.; Savateev, A.; Antonietti, M.; Wang, X. Tailoring the grain boundary chemistry of polymeric carbon nitride for enhanced solar hydrogen production and CO<sub>2</sub> reduction. *Angew. Chem. Int. Ed.* **2019**, *58*, 3433–3437. [[CrossRef](#)] [[PubMed](#)]
25. Zhang, G.; Zhu, J.; Xu, Y.; Yang, C.; He, C.; Zhang, P.; Li, Y.; Ren, X.; Mi, H. In-plane charge transport dominates the overall charge separation and photocatalytic activity in crystalline carbon nitride. *ACS Catal.* **2022**, *12*, 4648–4658. [[CrossRef](#)]
26. Zhai, B.; Li, H.; Gao, G.; Wang, Y.; Niu, P.; Wang, S.; Li, L. A crystalline carbon nitride based near-infrared active photocatalyst. *Adv. Funct. Mater.* **2022**, *32*, 2207375. [[CrossRef](#)]
27. Schwinghammer, K.; Hug, S.; Mesch, M.B.; Senker, J.; Lotsch, B.V. Phenyl-triazine oligomers for light-driven hydrogen evolution. *Energy Environ. Sci.* **2015**, *8*, 3345–3353. [[CrossRef](#)]
28. Burrow, J.N.; Ciufu, R.A.; Smith, L.A.; Wang, Y.; Calabro, D.C.; Henkelman, G.; Mullins, C.B. Calcium poly(heptazine imide): A covalent heptazine framework for selective CO<sub>2</sub> adsorption. *ACS Nano* **2022**, *16*, 5393–5403. [[CrossRef](#)]
29. Bojdys, M.J.; Müller, J.-O.; Antonietti, M.; Thomas, A. Ionothermal synthesis of crystalline, condensed, graphitic carbon nitride. *Chem.-Eur. J.* **2008**, *14*, 8177–8182. [[CrossRef](#)]
30. Lin, L.; Ou, H.; Zhang, Y.; Wang, X. Tri-s-triazine-based crystalline graphitic carbon nitrides for highly efficient hydrogen evolution photocatalysis. *ACS Catal.* **2016**, *6*, 3921–3931. [[CrossRef](#)]
31. Wang, X.; Chen, X.; Thomas, A.; Fu, X.; Antonietti, M. Metal-containing carbon nitride compounds: A new functional organic-metal hybrid material. *Adv. Mater.* **2009**, *21*, 1609–1612. [[CrossRef](#)]
32. Li, X.-H.; Antonietti, M. Metal nanoparticles at mesoporous N-doped carbons and carbon nitrides: Functional Mott–Schottky heterojunctions for catalysis. *Chem. Soc. Rev.* **2013**, *42*, 6593–6604. [[CrossRef](#)]
33. Zhu, X.; Zhang, T.; Sun, Z.; Chen, H.; Guan, J.; Chen, X.; Ji, H.; Du, P.; Yang, S. Black phosphorus revisited: A missing metal-free elemental photocatalyst for visible light hydrogen evolution. *Adv. Mater.* **2017**, *29*, 1605776. [[CrossRef](#)]
34. Tian, B.; Tian, B.; Smith, B.; Scott, M.C.; Lei, Q.; Hua, R.; Tian, Y.; Liu, Y. Facile bottom-up synthesis of partially oxidized black phosphorus nanosheets as metal-free photocatalyst for hydrogen evolution. *Proc. Natl. Acad. Sci. USA* **2018**, *115*, 4345–4350. [[CrossRef](#)]
35. Elbanna, O.; Zhu, M.; Fujitsuka, M.; Majima, T. Black phosphorus sensitized TiO<sub>2</sub> mesocrystal photocatalyst for hydrogen evolution with visible and near-infrared light irradiation. *ACS Catal.* **2019**, *9*, 3618–3626. [[CrossRef](#)]
36. Liang, Q.; Shi, F.; Xiao, X.; Wu, X.; Huang, K.; Feng, S. In situ growth of CoP nanoparticles anchored on black phosphorus nanosheets for enhanced photocatalytic hydrogen production. *ChemCatChem* **2018**, *10*, 2179–2183. [[CrossRef](#)]
37. Wen, M.; Wang, J.; Tong, R.; Liu, D.; Huang, H.; Yu, Y.; Zhou, Z.K.; Chu, P.K.; Yu, X.F. A low-cost metal-free photocatalyst based on black phosphorus. *Adv. Sci.* **2019**, *6*, 1801321. [[CrossRef](#)]
38. Zhu, M.; Osakada, Y.; Kim, S.; Fujitsuka, M.; Majima, T. Black phosphorus: A promising two dimensional visible and near-infrared-activated photocatalyst for hydrogen evolution. *Appl. Catal. B* **2017**, *217*, 285–292. [[CrossRef](#)]
39. Zhu, M.; Cai, X.; Fujitsuka, M.; Zhang, J.; Majima, T. Au/La<sub>2</sub>Ti<sub>2</sub>O<sub>7</sub> nanostructures sensitized with black phosphorus for plasmon-enhanced photocatalytic hydrogen production in visible and near-infrared light. *Angew. Chem. Int. Ed.* **2017**, *56*, 2064–2068. [[CrossRef](#)]

**Disclaimer/Publisher’s Note:** The statements, opinions and data contained in all publications are solely those of the individual author(s) and contributor(s) and not of MDPI and/or the editor(s). MDPI and/or the editor(s) disclaim responsibility for any injury to people or property resulting from any ideas, methods, instructions or products referred to in the content.